Article:
Dan, Y., Li, P., Holden, J. et al. (2025) PESERA-LP: A coarse-scale process-based fluvial erosion model for topographically complex regions. Journal of Hydrology, 655. 132923. ISSN: 0022-1694

https://doi.org/10.1016/j.jhydrol.2025.132923

PESERA-LP: A coarse-scale process-based fluvial erosion model for topographically complex regions

Yang Dan[a], Pengfei Li[a,*], Joseph Holden[b], Jinfei Hu[a], Brian Irvine[b], Qiong Wu[a], Jianjian Gao[c], Tianmin Dang[d], Guangju Zhao[e]

a. College of Geomatics, Xi'an University of Science and Technology, Xi'an 710054, China

b. water@leeds, School of Geography, University of Leeds, Leeds, LS2 9JT, UK

c. Suide Test Station of Soil and Water Conservation, Yellow River Conservancy Committee of Ministry of Water Resources, Yulin 719000, China

d. Yellow River Basin Monitoring Center of Water-Soil Conservation and Eco-Environment, Xi'an 710021, China

e. State Key Laboratory of Hydrology-Water Resources and Hydraulic Engineering, Nanjing Hydraulic Research Institute, Nanjing 210029, China

Corresponding author:

Pengfei Li, College of Geomataics, Xi'an University of Science and Technology, Xi'an 710054, China. Email: pengfeili@xust.edu.cn

Abstract:

The Chinese Loess Plateau, characterized by complex and fragmented topography, has undergone severe soil loss over the past century. While over thirty soil erosion models have been used in the region, most contemporary models are either catchment-scale or event-based. There is a notable absence

of regional-scale models that account for erosion-relevant processes specific to the Plateau. In this study, we developed a new scheme (PESERA-LP) for the simulation of soil erosion processes on the Loess Plateau. The model integrated advanced hydrological, vegetation, and erosion modules to enhance our understanding and prediction of soil erosion dynamics on the Plateau. In our scheme, the key parameter of the hydrological module was spatialized based on precipitation, while the terrain factor from the Revised Universal Soil Loss Equation (RUSLE) model and the erodibility factor of the Erosion Productivity Impact Calculator (EPIC) model were incorporated into the erosion module. Additionally, the parameters of the vegetation growth module were also optimized. PESERA-LP was implemented in both equilibrium and time-series modes, with a validation conducted based on field measurements. Validation of runoff depth in the equilibrium mode demonstrated a Root Mean Square Error (RMSE) of 0.47 mm a^{-1} and a Nash-Sutcliffe Efficiency (NSE) of 0.63, while the time-series mode exhibited an RMSE of 0.25 mm m^{-1} and an NSE of 0.58. As for erosion rate, RMSE and NSE were 6.04 t ha^{-1} a^{-1} and 0.89 in the equilibrium mode, compared to 0.99 t ha^{-1} m^{-1} and 0.52 in the time-series mode. Sensitivity analysis demonstrated that modelled runoff depth was sequentially impacted by precipitation, temperature, and vegetation cover, while modelled erosion rates were sequentially influenced by vegetation, precipitation, slope gradient, and temperature. The equilibrium mode is suitable for assessing spatial

variability of average erosion rates across large areas, whereas the time-series mode is preferentially used for analyzing continuous monthly erosion rates in relatively small areas.

Keywords: Erosion modelling; Regional scale; Process-based model; PESERA; Loess Plateau; Complex terrains.

1. Introduction

Accurate quantification of soil erosion over large areas is crucial for an in-depth understanding of erosion processes and the development of effective control strategies (Alewell et al., 2019; Borrelli et al., 2021). Soil erosion models exhibit advantages for large-scale assessments compared to other research methods (e.g. field monitoring, laboratory experiments etc.), particularly in evaluating long-term spatial patterns of erosion rates and predicting the response of erosion processes to different climate change and land-use change scenarios (Borrelli et al., 2017; de Vente et al., 2013; García-Ruiz et al., 2015). Hence, soil erosion models have become an increasingly vital tool since the 1980s (Panagos et al., 2015).

Although various soil erosion models have been developed, most of them were designed for catchment-scale and event-based simulations, focusing on specific catchments (Alewell et al., 2019). Notable examples include the Water

Erosion Prediction Project (WEPP) (Laflen et al., 1991), the Limburg Soil Erosion Model (LISEM) (De Roo et al., 1996), and the Rangeland Hydrology and Erosion Model (RHEM) (Hernandez et al., 2017). However, models that are suitable for regional-scale and long-term period simulations have been severely lacking.

Over the past five decades, the Universal Soil Loss Equation (USLE) (Wischmeier and Smith, 1978) and its modified versions have demonstrated robust applicability on a continental basis and for some global assessments, mainly owing to the advantages of their low input data requirement (Alewell et al., 2019). Despite the commendable accuracy of the USLE-series models, their empirical basis limits their ability to simulate dynamic erosion-related processes, further constraining their use in scenario studies. Additionally, these models do not account for agricultural practices such as crop planting and harvesting, thereby restricting their utility in modeling erosion under diverse crop management strategies (Alewell et al., 2019; Borrelli et al., 2021; Li et al., 2017).

In order to overcome the drawbacks of the USLE-series models, Kirkby et al. (2003) developed a regional-scale process-based pan-European Soil Erosion Risk Assessment (PESERA). The model integrates the interactions between runoff-generation processes and vegetation growth, which were then combined

with an erosion module (Li et al., 2017). The model assumed that the study area was composed of a cascade of slopes and did not consider the channel processes, facilitating the use of the model over large areas. Therefore, PESERA has presented a promising solution for large-scale erosion process modelling (Esteves et al., 2012; Karamesouti et al., 2016; Li et al., 2016b; Li et al., 2020). The model has been extensively applied across countries including the United Kingdom (Li et al., 2016b), Turkey (Cilek, 2017), the Netherlands (Wohler et al., 2021), and Greece (Karamesouti et al., 2015), and other countries across Europe (Kirkby et al., 2008). Li et al. (2016a) also incorporated freeze-thaw and desiccation processes into the model, significantly improving its applicability in blanket peatlands. However, Li et al. (2020) demonstrated that PESERA did not produce satisfactory results when applied to a complex terrain environment that was particularly susceptible to erosion, although it exhibited a good representation of vegetation.

The Chinese Loess Plateau has experienced the most severe soil erosion in the world, with erosion rates in some regions even exceeding 30,000 t km^{-2} a^{-1} (Chen et al., 2007; Sun et al., 2014). The erosion processes on the plateau, characterized by steep, highly varied slopes and deep gullies, are rather different from those on more uniform gently sloping areas (e.g. rill and interill erosion). From our literature evaluation we concluded that, to the best of our

knowledge, no regional-scale process-based models have been developed for the entire Loess Plateau due to the inability of existing models to adapt to the complex topography and diverse erosion processes. The PESERA model, with its process-based nature and capability for large-scale implementation, provides a promising solution for this challenge. However, as stated above, adaptations are needed for PESERA to improve its applicability to regions with complex terrain.

To address the challenges of simulating regional-scale soil erosion processes in the complex terrain environment, we developed a new scheme in this study - the PESERA-LP model - through heavily adapting the PESERA model. The objectives were: (1) to establish a parameterization strategy for key parameters in the hydrological module; (2) to improve the suitability of PESERA for complex terrain through incorporating the erodibility factor from the Erosion Productivity Impact Calculator (EPIC) model (Sharpley, 1990) and the topographic factor for steeply sloping conditions in the erosion module; (3) to localize parameters for crop growth cycles and actual-to-potential evapotranspiration ratios in the vegetation growth module; and (4) to calibrate and validate the PESERA-LP model with field measurements, followed by a comprehensive sensitivity analysis.

2. Study areas and data

2.1 Study areas

The Chinese Loess Plateau (33°41′ N-41°16′ N, 100°52′ E-114°33′ E) extends over an area of 635,000 km^2 in north-central China (Fig. 1). This region is one of the most severely eroded and ecologically fragile areas in the world (Zhang and Chen, 2020). The region, comprising plateaus, hills, and mountains, features a complex and fragmented topography, while elevations range from 85 m to 5210 m above sea level and slope gradients vary from 0% to 71% (Guan et al., 2021). The topography transitions from higher northwestern regions to lower southeastern areas, with the terrain predominantly comprising mountains and hills in the west and flatter landscapes in the east (Li et al., 2021b). The soil types of the Loess Plateau include dark loessial soils, loessial soils, and brown soils, among others (http://soil.geodata.cn). The most dominant and widely distributed soil type is the loessial soil, which is characterized by deep layers and a loose texture (Yu et al., 2020). The mean annual vegetation coverage on the Loess Plateau ranges from 0% to 68%, gradually increasing from northwest to southeast. The vegetation is predominantly composed of grasses and shrubs (Sun et al., 2014). The vegetation has been badly damaged due to prolonged excessive farming, overgrazing and continuous drought, leading to severe degradation on some areas (He et al., 2021). Especially in the hilly and gully

areas, the vegetation cover is relatively low and the protection of the soil is weak (Jin et al., 2021). The plateau is within the monsoon zone, where annual precipitation varies from 150 mm in the northwest to 700 mm in the southeast, and mean annual temperatures range from 4.3°C in the northwest to 14.3°C in the southeast (Zhao et al., 2013). The region experiences intense summer precipitation that can erode unprotected land surfaces (Tang and Sui, 2022; Tang et al., 2023). Since the 1970s, large conservation measures (terraces, check dams, vegetation restoration) have been implemented to reduce erosion intensity on the Loess Plateau (Li et al., 2017). Erosion rates on the Plateau have thus been dramatically decreased. However, large areas are still at a severe risk of erosion, particularly given the frequent occurrence of intensive rainstorms in the last decade (Li et al., 2022).

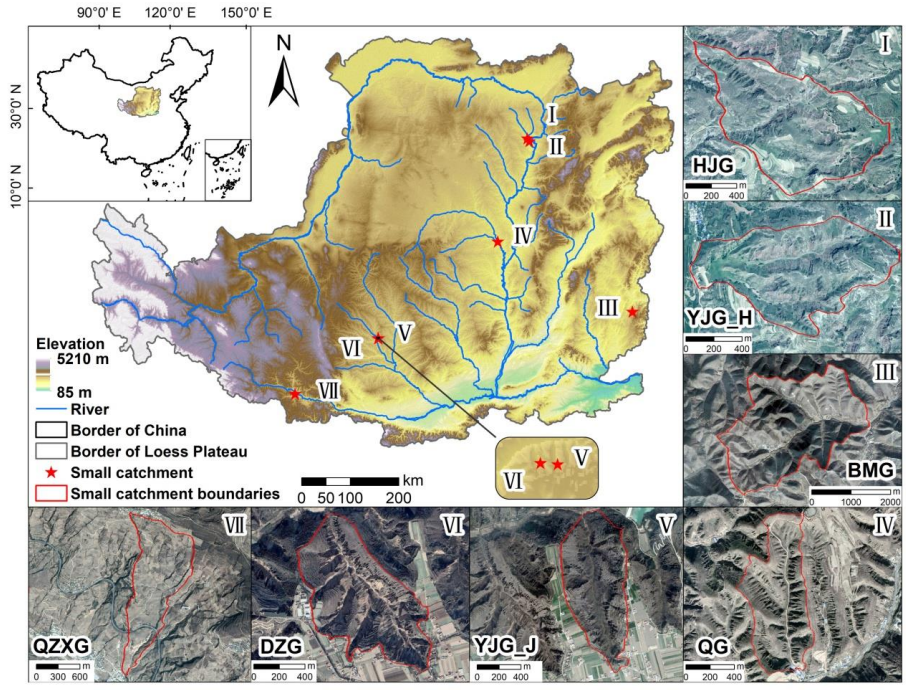

Fig.1 Overview of the study site, including elevation of the Loess Plateau and satellite

159 images for the seven small-scale catchments used for the development and validation of
160 PESERA-LP. The catchments are labeled as follows: I. Huangjiagou (HJG), II.
161 Yangjiagou_Huangfuchuan (YJG_H), III. Baimagou (BMG), IV. Qiaogou (QG), V.
162 Yangjiagou_Jinghe (YJG_J), VI. Dongzhuanggou (DZG), and VII. Qiaozixigou (QZXG).

163 ## 2.2 Data Collection and Preprocessing

164 ### 2.2.1 Field data for model development

165 We conducted a comprehensive literature search on China's National
166 Knowledge Infrastructure (CNKI) and the Web of Science (WOS) based on the
167 key words of 'Loess Plateau', 'small catchment', 'runoff' and 'soil erosion'. We
168 focused on studies on the Loess Plateau since 2000, mainly because of the
169 availability of vegetation coverage data (e.g. Moderate Resolution Imaging
170 Spectroradiometer (MODIS)) that were crucial for model development and
171 implementation. As a result, 165 papers were obtained. They were then
172 screened to collect runoff depth and erosion rate data.

173

174 Several criteria were set in terms of selecting relevant data for model
175 development and validation: (1) relatively small catchments (< 6 km^2) located
176 on the Loess Plateau were preferred; (2) no anthropogenic interventions such
177 as reservoirs or silt dams were found in the small catchments; (3) the monitoring
178 information for the small catchment contained, or can be converted to, runoff

and sediment related data. Relatively small catchments with limited interventions were selected in order to ensure that the measured data at catchment outlets were representative of erosion rates. Based on these criteria, 37 annual datasets from seven typical small catchments were obtained. Additionally, twelve monthly datasets spanning one year for one of these catchments were also included (Table 1). The catchments (Fig. 1) included Huangjiagou (HJG), Yangjiagou_Huangfuchuan (YJG_H), Qiaogou (QG), Dongzhuanggou (DZG), Yangjiagou_Jinghe (YJG_J), Qiaozixigou (QZXG), and Baimagou (BMG). The dataset contained measured runoff depths and erosion rates from different locations and dates on the Loess Plateau. The data were sourced from gauging stations in experimental catchments/watersheds. Quality control measures were applied during data processing, including consistency checks and outlier detection (Table 1). Among the datasets, 80 % were used for model development, while the remaining 20% were used for model validation. Specifically, 29 annual datasets were used for model construction and calibration, while the remaining eight annual datasets, along with the monthly data described above, were used for model validation.

196 **Table 1** Basic information for the small catchments used for model development and validation

Name	Location	Area	Soil type	Vegetation coverage (%)	Precipitation range (mm/a)	Slope gradient range (%)	Data period	Validation time	Type	Quality	Source
HJG	39°23′53″–39°24′36″N 111°0′40″–111°1′47″E	1.04 km^2	Dark loessial soils	10.44-23.61	239.0-646.9	0.62-20.86	2001 - 2012	2004, 2007	Annual	Q1[a]	(Li, 2016)
YJG_H	39°20′44″–39°21′14″N 111°3′31″–111°4′30″E	0.69 km^2	Dark loessial soils	20.40-21.70	286.9-559.9	1.47-14.82	2007 - 2010	2009	Annual	Q1	(Zhao et al., 2017)
QG	37°29′36″–37°30′16″N 110°17′23″–110°17′48″E	0.45 km^2	Loessial soils	24.13-27.56	375.4-398.2	0.96-18.67	2000-2005 average, 2000-2008 average	2000-2008 average	Annual	Q2[b]	(Liu et al., 2022; Wang, 2017)
DZG	35°41′20″–35°42′09″N 107°32′23″–107°33′14″E	1.15 km^2	Loessial soils	20.40-21.70	391.3-614.5	0.20-31.94	2005 - 2010	2007	Annual	Q1	(Guo, 2022)
YJG_J	35°41′14″–35°42′11″N 107°33′03″–107°33′38″E	0.87 km^2	Loessial soils	54.12-59.95	391.3-577.1	0.10-33.02	2006 - 2009	2007	Annual	Q1	(Guo, 2022)
QZXG	34°36′19″–34°37′29″N 105°42′18″–105°42′56″E	1.09 km^2	Loessial soils	30.60-45.02	462.5-867.2	6.11-27.06	2001, 2003, 2004	2003	Annual	Q2	(Chen, 2008)
BMG	36°07′29″–36°09′6″N 113°20′30″–113°22′56″E	5.76 km^2	Brown soils	58.13-68.19	421.8-687.2	0.32-27.70	2009 - 2014	2012	Annual	Q1	(Gao, 2017)
QZXG	34°36′19″–34°37′29″N 105°42′18″–105°42′56″E	1.09 km^2	Loessial soils	-	-	6.11-27.06	2003.1 - 2003.12	2003.1 - 2003.12	Monthly	Q2	(Chen, 2008)

197 [a] Q1: Data estimated from figures in papers. When data were presented only in graphical form, we employed the GetData Graph Digitizer software to derive estimates.

[b] Q2: Data directly extracted from papers. This represents data points that were explicitly provided in text or tables.

198 2.2.2 Input data for PESERA

199 In this study, all model runs were performed with a spatial resolution of 100 m,
200 which was similar to the length of slopes on the Loess Plateau. The PESERA
201 model required 128 layers of input data (Kirkby et al., 2003; Li et al., 2016b),
202 which were categorized into meteorological data, land use / cover data, soil
203 data and topographic data. The daily value dataset (V 3.0) of China's surface
204 climate data from China Meteorological Administration (CMA)
205 (https://data.cma.cn/) was used to obtain meteorological data. A total of 212
206 stations were selected from the dataset in and around the Loess Plateau,
207 including data on maximum temperature, minimum temperature, mean
208 temperature, precipitation, wind speed, sunshine hours, and relative humidity.
209 In addition, Potential Evapotranspiration (PET) was estimated using Penman's
210 formula (Valiantzas, 2013) based on maximum temperature, minimum
211 temperature, daily mean temperature, wind speed and direction, sunshine
212 duration and relative humidity data. Finally, these data were fitted and
213 interpolated into 100 m resolution raster data by applying the ANUSPLIN
214 software package with the partial thin-plate smooth spline method, which has
215 been widely used in related fields (Hutchinson, 1992).
216
217 Land-use data were obtained from the Resource and Environment Science and

Data Centre (RESDC) and were available every five years. Vegetation cover was calculated based on MODIS NDVI data provided by the National Aeronautics and Space Administration (NASA). For crops, the information was obtained from the statistical yearbook published by the National Bureau of Statistics (NBS) (http://www.stats.gov.cn/), and the tillage data were provided by the official websites of the regional agricultural bureaus. Soil attribute data were taken from the China Soil Attribute Dataset (CSAD) developed by Beijing Normal University (Shangguan et al., 2013), which was specifically used for land surface modelling studies. The terrain data were adopted from the SRTM (Shuttle Radar Topography Mission) data product (https://srtm.csi.cgiar.org/) with a 90 m resolution. All of the above data were resampled to 100 m resolution for modelling run consistency.

3. Overview and adaptations to PESERA

3.1 Original PESERA model

PESERA, operating on a monthly basis, is composed of a vegetation growth module, hydrological module and erosion module, taking account of the interaction among the processes. In addition, PESERA is capable of operating under different climate change and land-use change scenarios. A brief introduction to PESERA is given below, while a more detailed description can be found in Kirkby et al. (2008) and Li et al. (2016b).

3.1.1 Hydrological module

The hydrological module is based on the hydrological balance, which separates precipitation (Pre) into the four main hydrological components of overland flow, subsurface flow, changes in soil moisture and evapotranspiration (ET) (Berberoglu et al., 2020). Surface flow (R_o), the dominant driver of soil erosion，is generated under two key hydrological conditions: when precipitation intensity surpasses the soil infiltration capacity and when excess overland flow results from soil saturation. R_o is quantitatively expressed as:

$$R_O = P(Pre - \mu) \quad (1)$$

where, μ is the runoff depth threshold (mm), being the lesser of the available near-surface water storage depending on soil texture and the sub-surface saturation deficit. P is the proportion of precipitation exceeding the runoff depth threshold that is converted to surface runoff.

Subsurface flow and changes in soil moisture are dynamically simulated by TOPMODEL (Beven and Kirkby, 1979), using topographic data, soil parameters, and climatic data. Subsurface flow mainly affects the water infiltration process, while changes in soil moisture reflect the accumulation and flow of water in the soil after precipitation. Soil moisture content is also an important basis for vegetation growth and surface runoff. ET, including plant transpiration and soil evaporation, is calculated from soil water content, root-depth ratio and potential

evapotranspiration. ET drives plant growth and soil organic matter changes, while the dynamics of vegetation and organic matter control soil water storage. Furthermore, PESERA also considers the effects of snow and permafrost on hydrological processes in cold climates, increasing the adaptability to extreme climatic conditions.

3.1.2 Vegetation growth module

The vegetation module is closely coupled with the hydrological module, jointly influencing the soil erosion process. The module estimates gross primary productivity, vegetation coverage, and soil organic matter based on a biomass carbon balance. Gross primary productivity is estimated as a proportion of the actual transpiration from the plant, and then offset by respiration, which increases exponentially with temperature and proportional to vegetation biomass. Leaf fall fraction is a decreasing function of biomass, and, for deciduous plants, extra leaf fall is achieved at a rate that increases with temperature if respiration is greater than gross primary productivity. Soil organic matter increases with leaf fall, and decomposes at a rate increasing with temperature. Cover converges on an equilibrium value, which is defined as the ratio of plant transpiration to PET, at a rate that is larger where biomass is small. The module also takes account of the harvesting of crops through their effects on vegetation coverage and biomass, as well as changes in water use

efficiency throughout the crop growth cycle.

The vegetation growth module is deeply coupled with the runoff production module. Firstly, vegetation growth is supported by plant transpiration that is derived based on the soil moisture deficit. Vegetation growth also directly affects runoff depth through precipitation interception and transpiration, both of which are quantified based on the biomass of the vegetation. Concurrently, the model accommodates vegetation root systems that enhance soil structure and the accumulation of leaf litter that boosts soil organic matter. These processes alter the soil's physical and hydrological properties, affecting the infiltration capacity and organic matter content of the soil, thereby indirectly affecting runoff production. In addition, vegetation growth also affects erosion processes through adjusting soil erodibility.

3.1.3 Soil erosion module

In the erosion module, soil erosion rate (SE) is defined as the average rate at which sediment is transported to the bottom of a slope, provided there is an adequate supply of sediment. The runoff depth (R_O) is the primary driver of soil erosion rate in the model, which is estimated in conjunction with soil erodibility and topographic features,

$$\mathrm{SE} = {R_O}^2 TE \tag{2}$$

where T is the surface roughness (m), defined as the standard deviation of elevation within a specified area. E is the soil erodibility, which is weighted by the erodibility of bare ground and vegetated areas, with the soil erodibility of vegetated areas in the model being 10% of that of bare ground:

$$E = E_b(1 - COV) + 0.1E_bCOV \quad (3)$$

where E_b is the soil erodibility of bare ground, indicating the erosion potential of various soil types under standardized conditions. COV represents vegetation cover. The values of E_b are normally assigned with reference to the Pedotransfer rule (Le Bissonnais et al., 2005).

3.2 Adaptations to PESERA

To apply PESERA on the Loess Plateau, the following key challenges were faced: (i) on the Loess Plateau, the geographic features are highly spatially heterogeneous, such that a single value of a key parameter cannot support a satisfactory simulation of hydrological processes; (ii) the topography and soil erodibility factors in the original model were developed based on environmental conditions for Europe, which may not be applicable to some other regions; (iii) localization of parameters in the vegetation growth module may be needed as they have not yet been calibrated for the plateau. To overcome these challenges, several improvements were incorporated, including the spatialization of a key hydrological parameter, adaptation of the erosion module

to more complex topographic and soil conditions, and localization of vegetation growth parameters. In line with these improvements, a new scheme of PESERA for the Loess Plateau (PESERA for Loess Plateau, PESERA-LP) was thus proposed (Fig. 2).

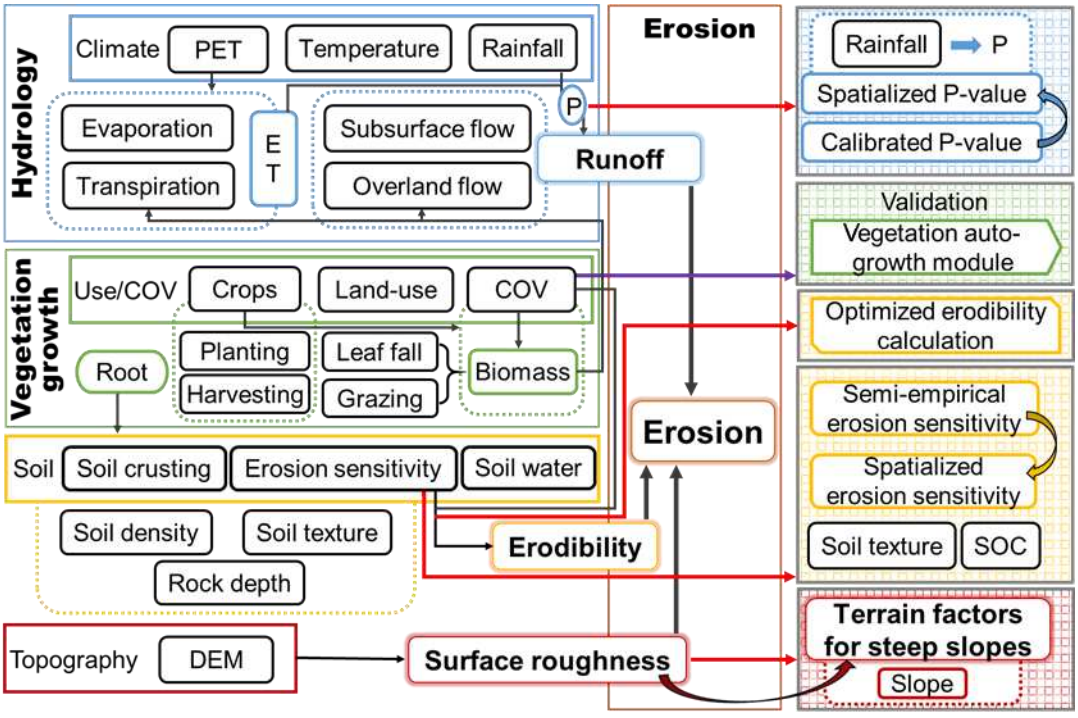

Fig.2 The framework of PESERA-LP. Boxes without shaded background represent the components directly inherited from the original PESERA model, while boxes with a shaded background indicate the adapted hydrology and erosion modules and the validation of the vegetation growth module in PESERA-LP.

3.2.1 Localization of the hydrological module

In the hydrological module, P is a crucial parameter (Equation 1). Precise calibration of P is critical for modeling accuracy. However, a constant P value may not yield the desired simulation results at different locations within the

Loess Plateau. Therefore, it was necessary to spatialize P to reflect regional discrepancies. A model for P value estimation was constructed to account for the spatial variation of P through analyzing the correlation between P and an array of spatial environmental factors.

Specifically, the PESERA model was utilized to simulate the runoff depth that corresponded temporally and spatially with the measured data in the constructed database. The P values were accurately calibrated by comparing the simulation results with measured data. Following the calibration, a correlation analysis was undertaken between these P values and a range of environmental variables, including topographic factor (S), T, leaf area index (LAI), COV, sand (Sa), silt (Si), clay (Cl), soil organic carbon (SOC), E_b, precipitation (Pre), ET, and PET. Results demonstrated that among the environmental variables, the correlation coefficient (R) between precipitation and P values was the highest (0.60), exhibiting a statistically significant positive correlation ($p < 0.01$) (Fig. 3). Four functional models were established including linear, exponential, logarithmic, and power functions. Coefficient of determination (R^2), mean square error (MSE) and Akaike informativeness criterion (AIC) were employed to evaluate the efficiency of the models.

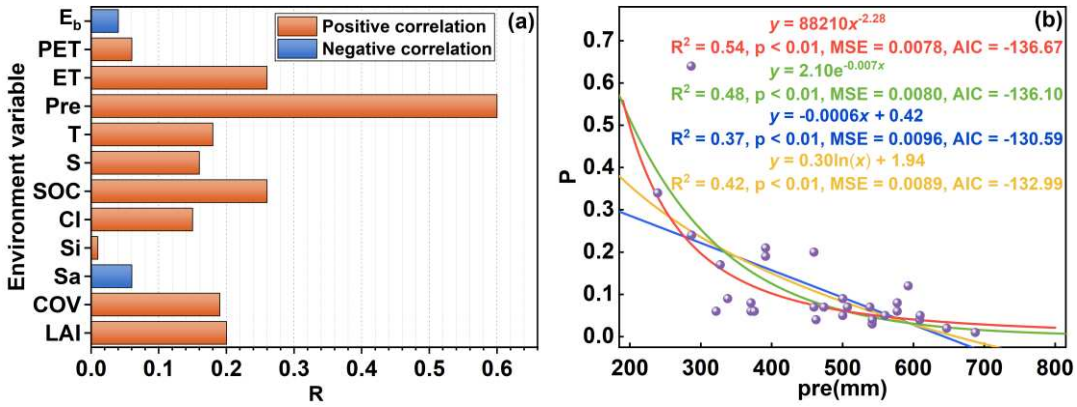

Fig.3 Construction of P value estimation models, including the correlation coefficient of P with environmental variables, including S, T, LAI, COV, Sa, Si, Cl, SOC, E_b, Pre, ET, PET (a) and four potential models (linear, exponential, logarithmic, and power) for deriving P values (b).

The R^2 quantifies how effectively the model captures the variability in the data, with values closer to 1 indicating superior explanatory power (Equation 4). The MSE assesses the discrepancy between the model predicted values and the actual observed values, with lower MSE values indicating higher accuracy (Equation 5). The AIC evaluates the trade-off between model complexity and fit quality, with lower AIC values implying that the model maintains good explanatory power while avoiding overfitting (Equation 6).

$$R^2 = 1 - \frac{\sum_{i=1}^{n}\left(O_i - \hat{O}_i\right)^2}{\sum_{i=1}^{n}(O_i - \bar{O})^2} \quad (4)$$

$$\mathrm{MSE} = \frac{1}{n}\sum_{i=1}^{n}(O_i - \hat{O}_i)^2 \quad (5)$$

$$\mathrm{AIC} = 2k - 2\ln(L) \quad (6)$$

where O_i is the optimal P-value obtained through calibration, $\hat{O}_i$ is the predicted value estimated through the established models, k represents the number of parameters in the model, and L is the likelihood function, which estimates how likely it is that the model would have produced the observed data.

The comprehensive assessment of these indicators demonstrated that the power function model outperformed the others (Fig. 3). The R^2 value of the power function model was the highest at 0.54 while its MSE value was the lowest at 0.0078, indicating that the model exerted the strongest ability to explain the data variability and superior prediction accuracy. In addition, the AIC value of the power function model was -136.67, which was lower than that of other models, suggesting that the model achieved the best fitting effect while maintaining lower model complexity. Therefore, the power function model was chosen to implement the spatialization of the P-value with the specific formula:

$$P = 88210pre^{-2.28} \quad (R^2 = 0.54, p < 0.01) \tag{7}$$

3.2.2 Adaptations to the erosion module

The Loess Plateau is characterized by deep gullies and steep-sloping areas, which presents difficulties for the use of PESERA, as demonstrated in Li et al. (2020). Therefore, it was necessary to incorporate the expression of steep slopes in the model. Moreover, the assignment of E_b (Equation 3) was based

on the pedotransfer rules established for European soils in the original erosion module, which was less practical and appropriate for the Loess Plateau. To address the challenges posed by the complex topography and erodibility derivation, we integrated the slope factor from the RUSLE model and the soil erodibility factor from the EPIC model (Sharpley, 1990) into the PESERA model to modify the T and E in the original model (Equations 2 and 3).

With regard to the sloping factor, Liu et al. (1994) adapted the terrain calculation formula established by McCool et al. (1987), thus significantly improving its suitability for the complex terrain environment. The formula described the relationship between soil loss and slope gradient on steep slopes exceeding 18%, integrating field data from the Loess Plateau. The formula used the sine of the slope angle as a key variable, which is physically representative of erosion processes. Therefore, the terrain factors were integrated into the PESERA model, with the specific formula being as follows:

$$\begin{cases} S = 10.8sin\theta - 0.03 & 0 < \theta < 9\% \\ S = 16.8sin\theta - 0.5 & 9\% \le \theta \le 18\% \\ S = 21.91sin\theta - 0.96 & 18\% < \theta \end{cases} \quad (8)$$

where θ is the slope.

The soil erodibility factor, quantified by the EPIC model, has been used and validated across a diverse range of geographical regions and soil types (Li et

al., 2022; Sun et al., 2014; Zhang et al., 2020). The methodology comprehensively reflected soil erodibility by incorporating key influencing parameters including soil texture, organic matter content, and soil saturation. The K_{EPIC} calculation is detailed as follows:

$$K_{EPIC} = \left\{0.2 + 0.3exp\left[0.0256Sa\left(1 - \frac{Si}{100}\right)\right]\right\}\left(\frac{Si}{Cl + Si}\right)^{0.3}\left(1 - \frac{0.25C}{C + \exp(3.72 - 2.95C)}\right)\left(1 - \frac{0.7SN}{SN + \exp(-5.51 + 22.9SN)}\right) \quad (9)$$

where C is the soil organic carbon content (%), Sa is the sand content (%), Si is the silt content (%), Cl is the clay content (%), and SN is the soil saturation, defined as SN = 1-Sa/100.

Furthermore, in order to improve the ability to simulate the impact of vegetation on soil erodibility, the formula for erodibility was redefined as $\mathrm{K} = f(COV, K_{EPIC})$. The K value was determined in terms of Equation 2, based on measured erosion rates and runoff depths, along with the S factors. Three vegetation expressions, COV, COV^2, and $\frac{COV}{1-COV}$ were evaluated to select the most effective form. These variants represented the basic vegetated cover, enhanced effects for higher coverage, and the ratio of vegetated areas to unvegetated areas, respectively. Functions were constructed using linear, exponential, logarithmic, and power functions to establish relationships between the various expressions for COV and K. The validity of these functions was assessed using R^2, MSE and AIC metrics. The results (Fig. 4)

demonstrated that these functions revealed a relatively low correlation with soil erodibility, with a highest R^2 of 0.45.

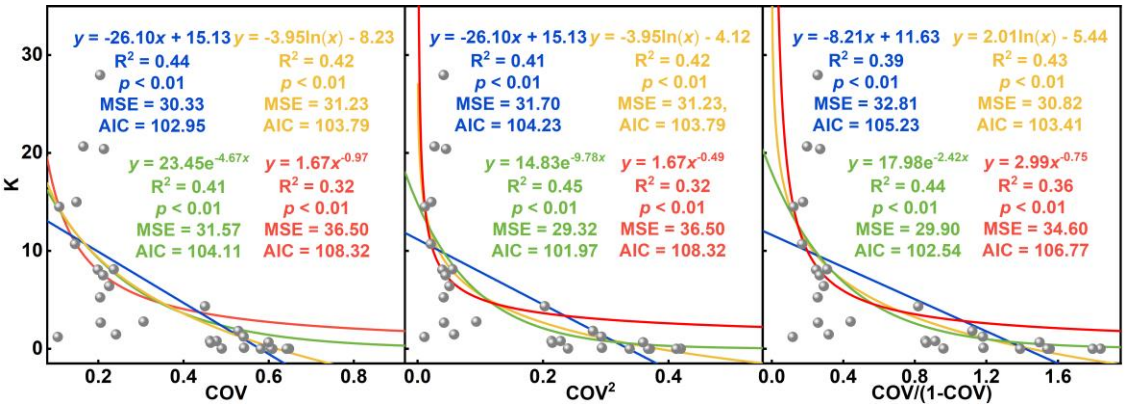

Fig.4 Comparative analysis of functional relationships between vegetation cover expressions (COV, COV^2, and $\frac{COV}{1-COV}$) and soil erodibility factor (K) using linear, exponential, logarithmic, and power models

Logarithmic transformations were applied to the independent variables, dependent variables and both of them separately to reduce the variance of data and diminish the effect of extreme values. Subsequently, linear regressions were employed to achieve the fitted models, which were then evaluated to achieve the best model.

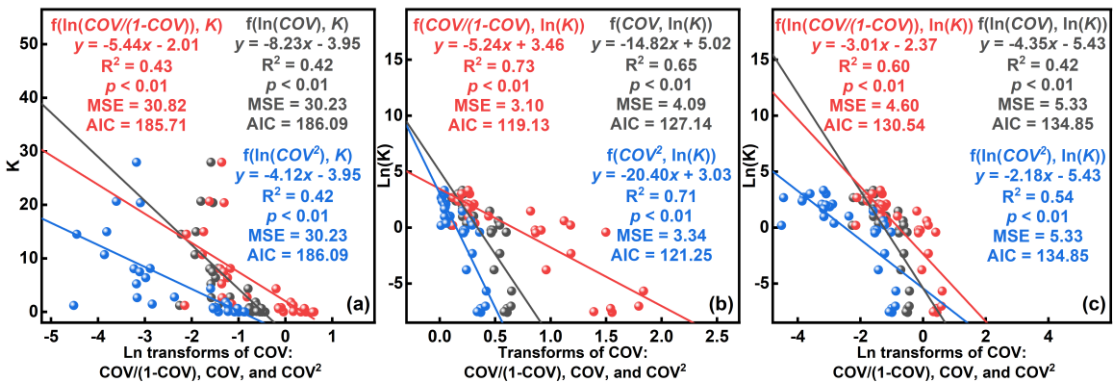

Fig.5 Linear regression analysis of logarithmically transformed vegetation cover expressions (COV, COV^2, and $\frac{COV}{1-COV}$) and K, including linear regression of logarithmically transformed vegetation cover expressions and K (a), vegetation cover expressions and logarithmically transformed K (b), and logarithmically transformed vegetation cover expressions and logarithmically transformed K (c).

The analysis indicated (Fig. 5) that the logarithmic transformation of the dependent variable, in conjunction with the $\frac{COV}{1-COV}$ expression for vegetation cover, yielded the most effective fit, achieving an R^2 of 0.73, an MSE of 3.1, and an AIC of 119.13. Based on these outcomes, the $\frac{COV}{1-COV}$ was chosen to represent the impact of vegetation on K. The constructed relationship was as follows:

$$\ln K = -5.2375 * \frac{COV}{1-COV} + 3.4592 \quad (10)$$

which was equivalent to:

$$K = 31.79 * e^{-5.24\left(\frac{COV}{1-COV}\right)} \quad (11)$$

Equation 11 illustrated that K varied with COV, reflecting the influence of vegetation coverage on soil erodibility. Additionally, K_{EPIC} represented the erodibility of bare soil, which was dependent on soil texture and organic carbon content. Theoretically, K equaled K_{EPIC} when vegetation cover was absent (0% COV). To integrate these factors, K was defined as:

$$K = f(K_{EPIC}) * f\left(\frac{\mathrm{COV}}{1-\mathrm{COV}}\right) \quad (12)$$

Based on Equations 11 and 12, $f\left(\frac{\mathrm{COV}}{1-\mathrm{COV}}\right)$ was expressed as:

$$f\left(\frac{\mathrm{COV}}{1-\mathrm{COV}}\right) = e^{-5.24\left(\frac{cov}{1-cov}\right)} \quad (13)$$

The function $f\left(\frac{\mathrm{COV}}{1-\mathrm{COV}}\right)$, which ranged from 0-1, quantified the impact of vegetation cover. Specifically, as vegetation cover approached 100%, the result of the equation was close to zero, indicating minimal soil erodibility. Conversely, at 0% vegetation cover, the function equaled 1, reflecting maximal soil erodibility.

Furthermore, we assumed that:

$$f(K_{EPIC}) = A + K_{EPIC} \quad (14)$$

where A is a constant representing the baseline erodibility, which varies according to different regions. In terms of Equation 11, the average erodibility for bare soil of the Loess Plateau was 31.79, while an average K_{EPIC} value for the region was calculated as 0.08. Consequently, the baseline value was deemed to be 31.71.

$$f(K_{EPIC}) = 31.79 - 0.08 + K_{EPIC} = 31.71 + K_{EPIC} \quad (15)$$

Therefore, the function f(K_{EPIC}) reflected a combination of baseline erosion levels and specific soil characteristics, indicating the erodibility under various soil conditions. Finally, a refined model was established to address both inherent soil characteristics and effects of vegetation:

$$K = (31.71 + K_{EPIC}) * e^{-5.24\left(\frac{cov}{1-cov}\right)} \quad (16)$$

3.2.3 Vegetation growth module parameterization

In the vegetation growth module, vegetation cover data are obtained through two methods: remote sensing and vegetation growth simulations. Remote sensing data, providing real-time, visual information, are suitable for erosion rate simulations during periods with available satellite data. Conversely, vegetation growth simulations are applied to historical period simulations and future scenario analyses in the absence of remote sensing data. However, the crop parameters used in the original vegetation growth model were not entirely suitable for the Loess Plateau. Thus, the parameters were localized to improve the applicability of the module.

Table 2 Growth cycle of dominant arable crop (months)

Dominant arable crop	Spring cereal	Winter cereal	Maize	Root crop	Oilseed
Growth cycle	4	9	4	6	5

In the study, crop growth cycles and evapotranspiration ratios (ET/PET) for different crops were adjusted. Crop growth cycles were used in the model to calculate crop planting and harvesting times, which were determined based on data published on the official website of the Department of Agriculture, China (https://ywglmh.moa.gov.cn/) (Table 2). The ET/PET ratio, a critical parameter for calculating vegetation evapotranspiration, was derived through spatial analysis methods that combined MODIS evapotranspiration data products with

land-use data (Table 3). These adjustments ensured that the model parameters were more closely aligned with actual vegetation growth conditions, thereby improving the applicability and accuracy of the model in historical simulations and future scenario projections.

Table 3 Monthly ET/PET ratios for individual crops on the Loess Plateau

Crop	Jan	Feb	Mar	Apr	May	Jun	Jul	Aug	Sep	Oct	Nov	Dec
Spring cereal	0.53	0.27	0.08	0.05	0.08	0.14	0.30	0.33	0.23	0.18	0.32	0.54
Winter cereal	0.52	0.35	0.15	0.14	0.16	0.16	0.24	0.33	0.35	0.29	0.37	0.51
Maize	0.61	0.35	0.12	0.06	0.07	0.11	0.19	0.28	0.22	0.23	0.36	0.62
Root crops	0.75	0.55	0.37	0.10	0.19	0.26	0.19	0.31	0.40	0.40	0.66	0.69
Oilseeds	0.50	0.41	0.24	0.17	0.17	0.23	0.34	0.34	0.32	0.27	0.38	0.51

3.2.4 Implementation of PESERA-LP

The PESERA-LP model adheres to the operational framework of the original PESERA model, providing both equilibrium and time series modes. In the equilibrium mode, the model uses multi-year average monthly data as inputs and, through an iterative process, reaches equilibrium to output average erosion rates as simulation results. The mode is primarily utilized for long-term assessment and extensive spatial analysis of soil erosion rates.

In contrast, the time-series mode requires detailed monthly data inputs to generate continuous monthly outputs, primarily focusing on the temporal dynamics of erosion rates and capturing extreme erosion events within the study period. However, the large data processing requirement associated with

518 the mode may become a limiting factor when applied to scenarios with high
519 spatial resolution and extensive scales. Consequently, the selection of an
520 appropriate mode is based on the study objectives, data availability and
521 computational capabilities needed before applying the PESERA-LP model.
522
523 As with the original PESERA, PESERA-LP also required 128 input layers.
524 However, the terrain factor and soil erodibility in PESERA-LP were derived
525 differently from the original PESERA (Equations 8 and 16).

526 3.2.5 Validation of PESERA-LP

527 Modelling results of PESERA-LP were compared with measured data to
528 validate the model performance and to assess the applicability of the model on
529 the Loess Plateau. The model results were evaluated using R^2, root mean
530 square error (RMSE) and Nash-Sutcliffe efficiency coefficient (NSE) to
531 quantitatively evaluate the model simulation accuracy in this study. The RMSE
532 and NSE were derived as follows and R^2 was calculated using Equation 4:

533 $$RMSE = \sqrt{\sum_{i=1}^{n} \frac{(S_i - O_i)^2}{n}} \quad (18)$$

534 $$NSE = 1 - \frac{\sum_{i=1}^{n}(O_i - S_i)^2}{\sum_{i=1}^{n}(O_i - \bar{O})^2} \quad (19)$$

535 where: O_i is measured values, S_i is simulated values, and $\bar{O}$ is the average
536 of observed values.

4. Model validation results

4.1 Equilibrium mode

The validation of the equilibrium mode of PESERA-LP was based on annual runoff and sediment datasets from the small catchments as well as annual MODIS vegetation cover data. Runoff depth modelling results exhibited an RMSE of 0.47 mm a^{-1} and an NSE of 0.63 (Fig. 6a). Similarly, the erosion module revealed a relatively high modelling precision, with an RMSE of 6.04 t ha^{-1} a^{-1} and an NSE of 0.89 (Fig. 6b). Modelled vegetation coverage of the localized vegetation growth module revealed a significant correlation with MODIS coverage, with an RMSE of 4.57% a^{-1} and an NSE of 0.30 (Fig. 6c).

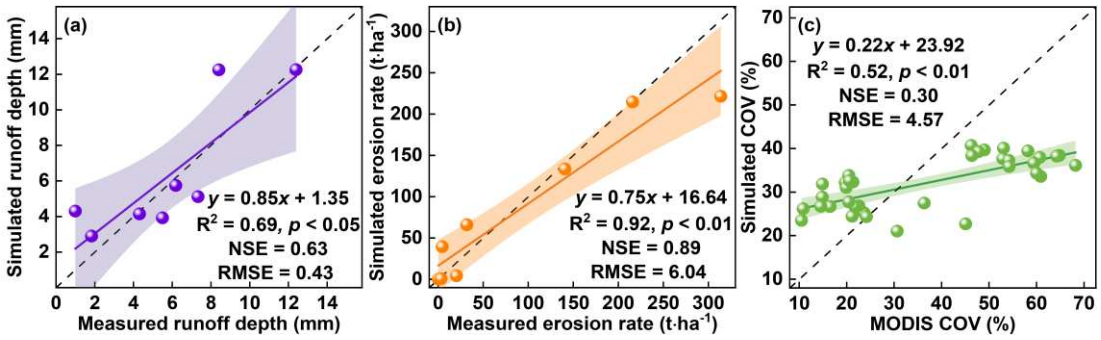

Fig.6 Validation of the equilibrium mode of PESERA-LP, including validation results for modelled runoff depth (a), modelled erosion rates (b) and modelled vegetation coverage (c).

4.2 Time-series mode

Monthly runoff depth and erosion rate data from the QZXG in 2003 were employed to evaluate the effectiveness of the hydrological and erosion modules.

Given the relatively small size of the QZXG area, a direct comparison of modelled monthly vegetation coverage and the relatively low resolution of MODIS results may result in considerable uncertainties. An indirect validation was conducted. Vegetation cover derived by the vegetation growth module was used to drive PESERA-LP, whilst the derived runoff depth and erosion rates were compared with field measurements.

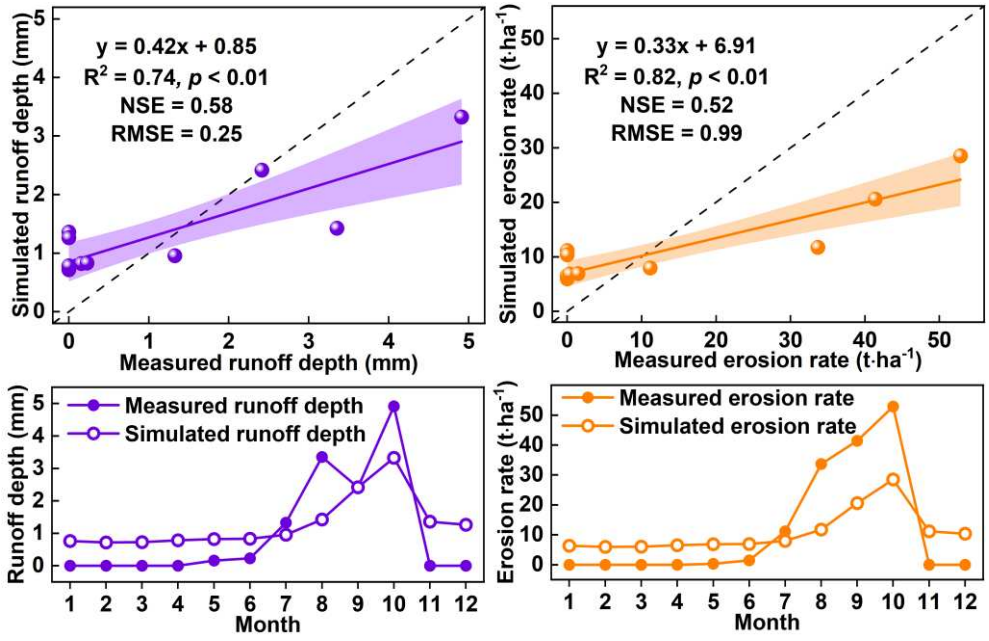

Fig.7 Validation of runoff depth and erosion rates modelled by the time-series mode of PESERA-LP with vegetation coverage derived from MODIS dataset, including scatter plots and line graphs for runoff depths and erosion rates validation.

The validation results showed that the model reliably simulated both runoff depths and erosion rates for the time-series mode. Specifically, the model exhibited a RMSE of 0.25 mm m^{-1} and an NSE of 0.58 for runoff depth

simulations, while for erosion rate simulations the validation results indicated an RMSE of 0.99 t ha^{-1} m^{-1} and an NSE of 0.52 (Fig. 7). A comparison of monthly simulation results with field measurements indicated that the model tended to overestimate lower values and underestimate higher ones for both runoff depth and erosion rate. Notably, during January to April and November to December, the model predicted non-zero values for both runoff depths and erosion rates, despite zero measurements being recorded during these periods. The peak values for both simulated runoff depths and erosion rates occurred in October, aligning with the seasonal variations observed in the actual data.

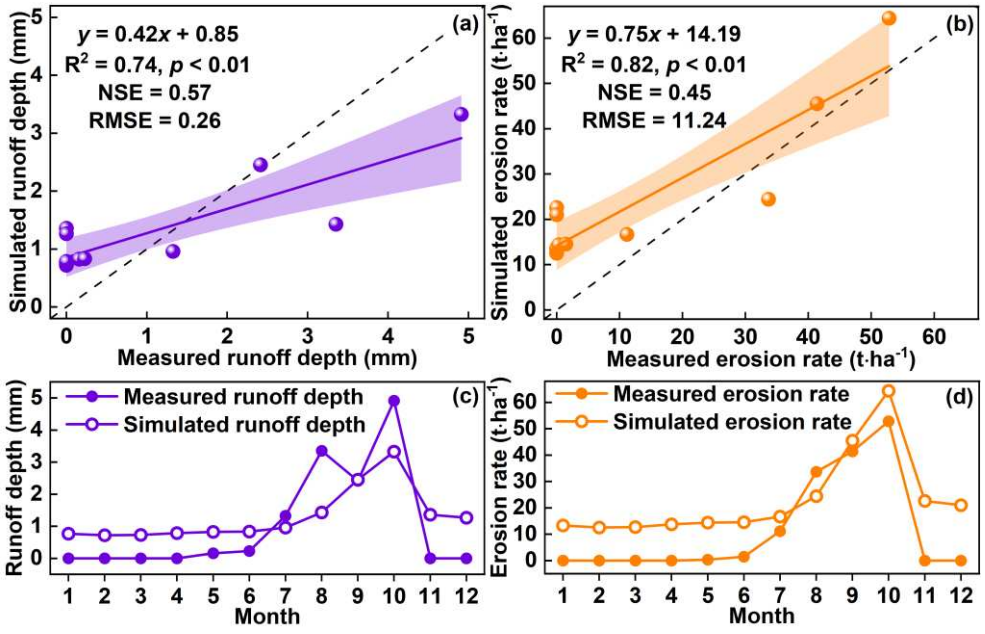

Fig.8 Validation of the PESERA-LP time-series mode with vegetation coverage generated by vegetation growth module, including scatter plots and line graphs comparing simulated runoff depths and erosion rates against measured data from January to December 2003

582 The indirect validation results (Fig. 8) revealed an RMSE of 0.26 mm m^{-1} for the
583 runoff depth and 11.24 t ha^{-1} m^{-1} for the erosion rate, with NSE values of 0.57
584 and 0.45, respectively. Modelling accuracy was generally comparable with the
585 results based on vegetation derived from MODIS datasets, although the
586 precision of erosion rate simulations slightly decreased. This demonstrated that
587 the modelling accuracy for the time-series mode of PESERA-LP for vegetation
588 was acceptable.

589 4.3 Sensitivity analysis

590 Sensitivity of PESERA-LP to crucial input variables, including precipitation,
591 temperature, topography and vegetation coverage, was investigated, taking the
592 conditions of HJG from 2001 to 2012 as a benchmark, which included a mean
593 annual precipitation of 403 mm, mean annual temperature of 8.71°C, mean
594 slope gradient of 7.98° and mean vegetation cover of 17.49%. The benchmark
595 value of parameters was adjusted separately to assess their impacts on
596 modelling results. The precipitation, temperature and slope gradient varied from
597 -100% to +100%, while vegetation cover varied from -100% to 0% at 10%
598 increments.

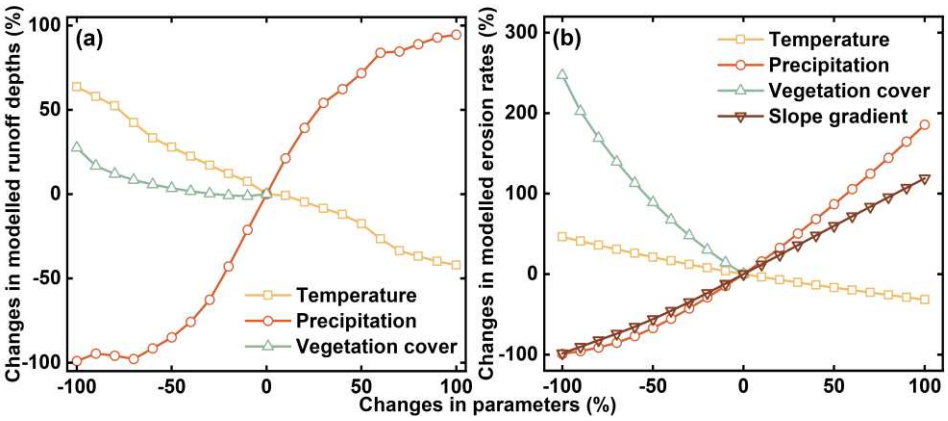

599

600 **Fig.9** Sensitivity analysis of PESERA-LP to key environmental parameters at HJG, 2001-
601 2012: sensitivity of runoff depths to changes in vegetation cover, precipitation, and
602 temperature (a); sensitivity of erosion rates to changes in slope gradient, vegetation cover,
603 precipitation, and temperature (b).

604

605 Results showed that modelled runoff depth decreased with increased
606 temperature and vegetation coverage. Modelled erosion rates increased with
607 rising precipitation and slope gradient and reduced with elevated temperature
608 and vegetation coverage. Notably, runoff depth was highly sensitive to changes
609 in precipitation; for instance, a 1.5-fold increase in precipitation significantly
610 amplified the modeled runoff depth by approximately 1.72-fold. Furthermore,
611 although temperature changes did impact the simulation outcomes, their
612 impacts on soil erosion rates were low compared to precipitation. Vegetation
613 cover exerted the lowest impact on modelled runoff production, compared to
614 precipitation and temperature. However, vegetation coverage exerted the
615 highest impact on modelled erosion rates, followed by precipitation, slope, and

temperature. Notably, reductions in vegetation did not only increase runoff depths but also exacerbated erosion rates. In extreme cases where vegetation was entirely absent, erosion rates were modelled to rise to nearly three times that of the benchmark.

5. Discussion

5.1 Advantages of the adapted modelling approach

PESERA-LP represents the first regional-scale process-based erosion model developed for the Loess Plateau. A comprehensive validation of the runoff module, erosion module and vegetation growth module showed that PESERA-LP had a high robustness for simulating both runoff depth and erosion rate on the Loess Plateau. The adapted model was able to reasonably simulate and predict both long-term average and continuous monthly erosion rates, demonstrating its capability for dynamic soil erosion scenario simulations. PESERA-LP is able to operate under different climate change and land-use change scenarios, providing an effective tool for assisting in the allocation of resources for soil and water resource conservation, which is crucial for the Loess Plateau (Jian et al., 2024; Zhai et al., 2023).

In our study, the critical parameter (P in Equation 1) of the hydrological module of PESERA was directly linked with precipitation, facilitating the large-scale

application of the model. On the Loess Plateau, precipitation is almost the only source for soil moisture (Jia et al., 2017), which implies that the intensity and /, or amounts of precipitation, should be important factors for the efficiency of precipitation converted to runoff, thereby implying that our results are reasonable. In addition, our scheme was not only beneficial for the use of PESERA over the Loess Plateau, but also provided a valuable reference for the calibration of other large-scale models over areas with highly varying environmental conditions.

Previous studies have demonstrated the limitations of the original PESERA to simulate erosion rates on steep slopes (Li et al., 2020). Topography is the primary factor affecting soil erosion rates on the Loess Plateau, especially on steep slopes exceeding 25 degrees, where erosion is the most serious (Sun et al., 2014; Xin et al., 2008). PESERA-LP has incorporated the adapted S factor of RUSLE that takes account of steeply sloping conditions. The model has been validated in typical small catchments of the plateau, showing a strong robustness and improved sensitivity to topography. In the original PESERA model, E_b was determined by classifying soils based on their particle size and assigning values to each category. However, the classification method exhibited considerable uncertainty when applied to wider regions, often requiring expert assessment to recalibrate E_b values, thus limiting the transferability of the

657 model. In our study, we incorporated the erodibility of the EPIC model (K_{EPIC}),
658 which can be quantitatively determined based on soil organic carbon and
659 particle size data, largely improving the applicability of the model.
660
661 Vegetation is a major influence on erosion rates of the Loess Plateau (Durán
662 Zuazo and Rodríguez Pleguezuelo, 2008; Zhang et al., 2022; Zhao et al.,
663 2022a). The relationship between COV and K was optimized through a
664 comparative analysis. The formula $\frac{COV}{1-COV}$ expressed the effect of COV on K,
665 effectively capturing the threshold and saturation effects of ecological
666 processes (Gao et al., 2023; Schmidt et al., 2018; Zhu et al., 2021). The
667 relationship between COV and soil erosion follows an exponential form (Elwell
668 and Stocking, 1976; Nunes et al., 2011). The exponential function effectively
669 captured the accelerated changes that occur in natural ecosystems
670 approaching threshold levels (Osterkamp et al., 2012), illustrating the nonlinear
671 relationship between COV and K (May, 1976). In this case, PESERA-LP is able
672 to reproduce real-world situations, where an increase of vegetation cover from
673 none to a moderate level significantly reduces soil erosion rates while the
674 protective effect of vegetation gradually decreases once the cover reaches a
675 critical threshold (Wang et al., 2016).

5.2 Comparative evaluation of model accuracy

Li et al. (2020) validated the original PESERA in the HJG and YJG_H catchments and found relative errors (RE) of 73.42% and 65.15% for modelled erosion rates (Table 4), which was considerably higher than that achieved in our study for PESERA-LP (13.98%,14.18%). An apparent decrease in the relative errors directly demonstrates the effectiveness of our modifications to PESERA.

Table 4 Comparison of PESERA-LP and the model performance of previous studies in the Loess Plateau

Source	Model	Small catchment	Period	RMSE	NSE	RE	RMSE (PESERA-LP)	NSE (PESERA-LP)	RE (PESERA-LP)
(Li et al., 2020)	PESERA	HJG, YJG_H	2001-2011 average	-	-	73.42 65.15	-	-	13.98 14.18
(Li et al., 2021a)	USLE	YJG_H, YJG_J, BM, HJG, DZG	2005,2010	29.76	0.20	-	10.01	0.73	-
(Li et al., 2022)	RUSLE	YJG_H, YJG_J, QG, BM, DZG, QZXG, HJG	2001-2014	33.91	0.16	-	7.26	0.56	-

USLE (Li et al., 2021a) and RUSLE (Li et al., 2022) have been the primary tools applied at large scales across the entire Loess Plateau. An accuracy comparison of our study with USLE / RUSLE results, in terms of RMSE and NSE demonstrated that PESERA-LP surpassed these models in simulating

690 erosion rates, as detailed in Table 4. Notably, unlike the empirically-based
691 USLE and RUSLE, PESERA-LP is capable of simulating runoff generation,
692 erosion rates and vegetation growth, providing more detailed insights into the
693 underlying processes.

694 5.3 Model sensitivity analysis

695 The sensitivity analysis of PESERA-LP indicated that increased precipitation
696 resulted in increased modelled runoff depth and soil erosion rates, which is
697 consistent with the conclusions obtained from the application of the PESERA
698 model in Turkey by Berberoglu et al. (2020). Modelled runoff production
699 increased rapidly with precipitation, with the changing rate being relatively low
700 at the highest and lowest range of precipitation. Such a phenomenon may be
701 attributed to the notion that precipitation tends to infiltrate when the soil is dry,
702 leading to low surface runoff production (Ma et al., 2022). As precipitation
703 continues to increase, the soil gradually reaches saturation, leading to a
704 decrease in infiltration rate. Consequently, a larger proportion of the
705 precipitation is converted into surface runoff, substantially increasing the
706 volume of runoff. As precipitation continues at a rate above the infiltration
707 capacity of the soil, a relatively stable surface runoff production ensues (Miao
708 et al., 2020).

709

Sensitivity analysis also demonstrated that increased vegetation coverage effectively reduced runoff depth and erosion rates, underscoring the critical role of vegetation in protecting soil erosion and water resources. Vegetation effectively intercepts precipitation through its cover and root structures, mitigating the direct impact of raindrops on the soil and thereby reducing the effects of splash erosion (Shi et al., 2022). Furthermore, the root systems of plants enhance the shear strength of soil and improve its permeability (Zhang et al., 2019), which reduces runoff depths and soil erosion rates (Gyssels et al., 2005).

In addition, sensitivity analyses also demonstrated that modelled erosion rates were rather sensitive to changes in slope gradients. Compared to the original PESERA, PESERA-LP exhibited enhanced sensitivity to changes in slope gradients. Given a benchmark slope gradient of 7.89, erosion rates predicted by the original PESERA increased by approximately 76% when the slope gradient doubled (Li et al., 2020), whereas PESERA-LP indicated an erosion rate increase of about 119%. This further confirms the feasibility of model adaptations compared to the original PESERA, better reflecting the role that topography plays in Loess Plateau erosion.

In contrast, temperature changes had a minor effect on modelled runoff depth

and modelled erosion rates, affecting runoff depth indirectly through changes in evapotranspiration. As temperatures rise, evapotranspiration generally increases, leading to a reduction in soil moisture and a subsequent decrease in surface runoff (Trenberth, 1999; Zhou et al., 2024). Additionally, temperature variations indirectly affect vegetation cover by altering plant growth conditions, which further affects erosion processes (Mondal and Mishra, 2024).

We also found that the sensitivity of soil erosion to vegetation cover was markedly greater than that to slope. This finding aligns with results from the analyses by Zhao et al. (2016) and Zhao et al. (2022b), based on field data from watersheds and plots in China. Those studies found that the correlation between vegetation cover and soil erosion was stronger than that with slope gradient. Meanwhile, it should be noted that the impacts of vegetation cover and slope gradient on soil erosion exhibited complex interactions, with sensitivity varying under diverse environmental conditions. Specifically, in regions with a higher vegetation cover, the sensitivity of soil erosion to slope gradient was relatively lower; conversely, in areas with a lower vegetation cover, the influence of slope gradient variations on soil erosion was more pronounced (He et al., 2023; Sun et al., 2021).

5.4 Limitations of the modelling approach

Our modelling approach is subject to several limitations. Firstly, although the vegetation growth module is able to simulate vegetation growth, the module is insufficiently parameterized to cover the full range of functional vegetation types, and is limited by absence or inadequate representation of some processes (e.g. fires) (Kirkby et al., 2008). This constrained the accuracy of the module. Therefore, when high-resolution remote sensing imagery is available, it is preferred in order to enhance the accuracy of modelling. The vegetation growth module, calibrated to global biomass data (Kirkby and Neale, 1987), is capable of dynamically simulating changes in vegetation cover while accounting for the characteristic stabilization of vegetation growth over time. However, the model lacks the capacity to capture the intricate dynamic processes in vegetation growth, including the effects of soil nutrients, moisture, and climatic conditions, which are not adequately reflected in the module. Consequently, the accuracy of vegetation cover simulation is relatively low in small-scale watershed validation. Future research could integrate soil and climatic conditions to optimize the model, thereby enhancing the simulation accuracy of dynamic changes in vegetation cover.

Secondly, in the model, individual storms are integrated over the frequency distribution of storms, which is substituted by the daily rainfall distribution. The

772 model estimates runoff production based on monthly average soil moisture,
773 which exhibits seasonal variations (Kirkby et al., 2008). This simplification
774 weakens the ability of PESERA to fully capture the dynamic impacts of
775 consecutive extreme rainfall events occurring over short periods. While this
776 may result in some loss of information, it effectively balances model accuracy
777 with computational efficiency. In semi-arid regions such as the Loess Plateau,
778 where soils typically remain dry between significant rainfall events (Shi et al.,
779 2011), the cumulative effects of consecutive rainfall events on runoff are
780 minimal. As a result, the use of monthly average soil moisture to estimate runoff
781 dynamics is not significantly compromised, minimizing the impact of information
782 loss. Therefore, although the model has limitations in simulating the impact of
783 high-intensity storms on soil erosion, particularly over short timescales, it
784 remains suitable for regional-scale erosion simulation, especially in regions
785 where soil moisture dynamics show a relatively weak response to short-term
786 extreme events.
787
788 Thirdly, the digital elevation model (DEM) used for PESERA-LP has a resolution
789 of 100 meters, derived from the 2000 NASA SRTM data. Although the resolution
790 is sufficient for simulating soil erosion at a regional scale, it may not fully capture
791 micro-topographic variations that could influence soil erosion (Chidi et al., 2021).
792 Future research could be undertaken using time-series topographic data that

reflect dynamic changes in topographic features (e.g. those derived using Synthetic Aperture Radar) to improve the accuracy of erosion predictions. In addition, PESERA-LP has the potential for application over wider regions. However, the applicability of PESERA-LP to other places outside the Loess Plateau requires further research and validation, given that the derivation method for key parameters of PESERA-LP (e.g. K in Equation 16) was developed specifically for the Loess Plateau environment.

Additionally, although we endeavored to collect datasets from different times and locations that met the criteria for the validation of the PESERA-LP model, the data used for model development were still limited, particularly by the absence of monthly and up-to-date measurements. Although validation results demonstrated the reliability of PESERA-PEAT, the precision of simulations within the time-series mode has been constrained. Underestimations of peak runoff depths and erosion rates in the time-series mode may stem from model development and calibration, which primarily relied on annual data rather than incorporating monthly measurements. Despite data from very recent years being unavailable, the data used in this study are representative and sufficiently reliable for the scope of the research. Nonetheless, the incorporation of more up-to-date data is desirable. In the future, more effort is required to collect field data for further validation and improvement of PESERA-LP.

Datasets included the effects of mass movements on steep slopes. However, a separate measurement for mass movement was rather rare, making an explicit integration of mass movement processes impossible. Remote sensing technologies, such as unmanned aerial vehicle (UAV) light detection and ranging (LiDAR) and structure from motion (SfM) photogrammetry, allow rapid monitoring of soil erosion (e.g. mass movement) over relatively large areas (Li et al., 2024; Li et al., 2023), providing a promising way of explicitly incorporating mass movement processes. In addition, the established model currently does not include routing algorithms, limiting its use for modelling sediment transport over landscapes. In the future, sediment transport algorithms should also be incorporated into the model to improve the capability of process description in the model.

6. Conclusions

In this study, the PESERA-LP model was developed as a new scheme specifically tailored for topographically complex regions. In PESERA-LP, the crucial parameter of the hydrological module was spatialized through its relation with precipitation. A slope factor for steeply-sloping conditions was incorporated to account for complex terrain. Erodibility was refined through integrating the erodibility factor of the EPIC model and a reasonable expression of impacts of

vegetation coverage. The hydrological, erosion and vegetation growth modules of the PESERA-LP model were validated based on field measurements in the equilibrium and time series modes, respectively, demonstrating that the model was applicable across the Loess Plateau. PESERA-LP, when operated in equilibrium mode, was adept at assessing the long-term impacts of erosion across vast areas with high spatial resolution. In time-series mode, it was appropriate for evaluating continuous monthly erosion risks and the effects of extreme events such as heavy rainfall and droughts. The development of PESERA-LP provides a good reference for use and adaptation of a regional-scale, process-based erosion model for other parts of the world. In the future, further effort should be made to incorporate more erosion processes in the model (e.g. mass movement, sediment transport). More field measurements should also be collected through various methods to facilitate refinement of the model.

7. Acknowledgements

This paper was financially supported by the National Natural Science Foundation of China (U2243211, 42207407), Major Science and Technology Program of the Ministry of Water Resources of China (SKS-2022092), and the ‘scientists +engineers’ team development project of Yulin High Tech Industrial Development Zone (YGXKG-2023-105).

8. References

Alewell, C., Borrelli, P., Meusburger, K., Panagos, P., 2019. Using the USLE: Chances, challenges and limitations of soil erosion modelling. International Soil and Water Conservation Research, 7(3): 203-225. DOI:https://doi.org/10.1016/j.iswcr.2019.05.004

Berberoglu, S., Cilek, A., Kirkby, M., Irvine, B., Donmez, C., 2020. Spatial and temporal evaluation of soil erosion in Turkey under climate change scenarios using the Pan-European Soil Erosion Risk Assessment (PESERA) model. Environmental Monitoring and Assessment, 192(8). DOI:https://doi.org/10.1007/s10661-020-08429-5

Beven, K.J., Kirkby, M.J., 1979. A physically based, variable contributing area model of basin hydrology. Hydrological sciences journal, 24(1): 43-69. DOI:https://doi.org/10.1080/02626667909491834

Borrelli, P., Alewell, C., Alvarez, P., Anache, J.A.A., Baartman, J., Ballabio, C., Bezak, N., Biddoccu, M., Cerdà, A., Chalise, D., 2021. Soil erosion modelling: A global review and statistical analysis. Science of the Total Environment, 780: 146494. DOI:https://doi.org/10.1016/j.scitotenv.2021.146494

Borrelli, P., Robinson, D.A., Fleischer, L.R., Lugato, E., Ballabio, C., Alewell, C., Meusburger, K., Modugno, S., Schütt, B., Ferro, V., Bagarello, V., Van Oost, K., Montanarella, L., Panagos, P., 2017. An assessment of the global impact of 21st century land use change on soil erosion. Nature Communications, 8. DOI:https://doi.org/10.1038/s41467-017-02142-7

Chen, L., Wei, W., Fu, B., Lü, Y., 2007. Soil and water conservation on the Loess Plateau in China: review and perspective. Progress in Physical Geography, 31(4): 389-403. DOI:https://doi.org/10.1177/0309133307081290

Chen, Y., 2008. Vegetation-erosion dynamic process research in typical watershed in the loess plateau. Doctoral Thesis, Beijing Forestry University.

Chidi, C.L., Zhao, W., Chaudhary, S., Xiong, D.H., Wu, Y.H., 2021. Sensitivity Assessment of Spatial Resolution Difference in DEM for Soil Erosion Estimation Based on UAV Observations: An Experiment on Agriculture Terraces in the Middle Hill of Nepal. Isprs International Journal of Geo-Information, 10(1). DOI:https://doi.org/10.3390/ijgi10010028

Cilek, A., 2017. Soil organic carbon losses by water erosion in a Mediterranean watershed. Soil Research, 55(4): 363-375. DOI:https://doi.org/10.1071/sr16053

de Vente, J., Poesen, J., Verstraeten, G., Govers, G., Vanmaercke, M., Van Rompaey, A., Arabkhedri, M., Boix-Fayos, C., 2013. Predicting soil erosion and sediment yield at regional scales: Where do we stand? Earth-Science Reviews, 127: 16-29. DOI:https://doi.org/10.1016/j.earscirev.2013.08.014

Durán Zuazo, V.H., Rodríguez Pleguezuelo, C.R., 2008. Soil-erosion and runoff prevention by plant covers: a review. Agronomy for Sustainable Development, 28: 65-86. DOI:https://doi.org/10.1051/agro:2007062

Elwell, H.A., Stocking, M.A., 1976. Vegetal cover to estimate soil erosion hazard in Rhodesia. Geoderma, 15(1): 61-70. DOI:https://doi.org/10.1016/0016-7061(76)90071-9

Esteves, T.C.J., Kirkby, M.J., Shakesby, R.A., Ferreira, A.J.D., Soares, J.A.A., Irvine, B.J., Ferreira, C.S.S.,

Coelho, C.O.A., Bento, C.P.M., Carreiras, M.A., 2012. Mitigating land degradation caused by wildfire: application of the PESERA model to fire-affected sites in central Portugal. Geoderma: An International Journal of Soil Science, 191: 40-50. DOI:https://doi.org/10.1016/j.geoderma.2012.01.001

Gao, L., 2017. Research on the soil and water conservation ecological effects at slope and small watershed scales in the rocky mountain areas of northern china. master Thesis, Beijing Forestry University. DOI:https://doi.org/10.26949/d.cnki.gblyu.2017.000891

Gao, S., Zhong, R., Yan, K., Ma, X., Chen, X., Pu, J., Gao, S., Qi, J., Yin, G., Myneni, R.B., 2023. Evaluating the saturation effect of vegetation indices in forests using 3D radiative transfer simulations and satellite observations. Remote Sensing of Environment, 295: 113665. DOI:https://doi.org/10.1016/j.rse.2023.113665

García-Ruiz, J.M., Beguería, S., Nadal-Romero, E., González-Hidalgo, J.C., Lana-Renault, N., Sanjuán, Y., 2015. A meta-analysis of soil erosion rates across the world. Geomorphology, 239: 160-173. DOI:https://doi.org/10.1016/j.geomorph.2015.03.008

Guan, Y., Yang, S., Zhao, C., Lou, H., Chen, K., Zhang, C., Wu, B., 2021. Monitoring long-term gully erosion and topographic thresholds in the marginal zone of the Chinese Loess Plateau. Soil and Tillage Research, 205: 104800. DOI:https://doi.org/10.1016/j.still.2020.104800

Guo, X., 2022. Response of runoff and sediment process to different vegetation on the Loess Plateau. master Thesis, Northwest A&F University. DOI:https://doi.org/10.27409/d.cnki.gxbnu.2022.001360

Gyssels, G., Poesen, J., Bochet, E., Li, Y., 2005. Impact of plant roots on the resistance of soils to erosion by water: a review. Progress in physical geography, 29(2): 189-217. DOI:https://doi.org/10.1016/B978-0-12-820106-0.00016-6

He, L., Lu, S., Wang, C., Mu, J., Zhang, Y., Wang, X., 2021. Changes in soil organic carbon fractions and enzyme activities in response to tillage practices in the Loess Plateau of China. Soil and Tillage Research, 209: 104940. DOI:https://doi.org/10.1016/j.still.2021.104940

He, Q., Li, B., Zhang, F., Shen, N., Yang, M., 2023. Optimal clipping intensity for balancing soil erosion control and runoff production on revegetated slopes. Journal of Hydrology, 620. DOI:https://doi.org/10.1016/j.jhydrol.2023.129470

Hutchinson, M., 1992. Documentation for SPLINA and SPLINB—Two Programs in the ANUSPLIN Software Package. Centre for Resource and Environmental Studies, Australian National University.

Jia, X.X., Shao, M.A., Zhu, Y.J., Luo, Y., 2017. Soil moisture decline due to afforestation across the Loess Plateau, China. Journal of Hydrology, 546: 113-122. DOI:https://doi.org/10.1016/j.jhydrol.2017.01.011

Jian, Z., Sun, Y., Wang, F., Zhou, C., Pan, F., Meng, W., Sui, M., 2024. Soil conservation ecosystem service supply-demand and multi scenario simulation in the Loess Plateau, China. Global Ecology and Conservation, 49. DOI:https://doi.org/10.1016/j.gecco.2023.e02796

Jin, F., Yang, W., Fu, J., Li, Z., 2021. Effects of vegetation and climate on the changes of soil erosion in the Loess Plateau of China. Science of The Total Environment, 773: 145514. DOI:https://doi.org/10.1016/j.scitotenv.2021.145514

Karamesouti, M., Detsis, V., Kounalaki, A., Vasiliou, P., Salvati, L., Kosmas, C., 2015. Land-use and

land degradation processes affecting soil resources: Evidence from a traditional Mediterranean cropland (Greece). Catena, 132: 45-55. DOI:https://doi.org/10.1016/j.catena.2015.04.010

Karamesouti, M., Petropoulos, G.P., Papanikolaou, I.D., Kairis, O., Kosmas, K., 2016. Erosion rate predictions from PESERA and RUSLE at a Mediterranean site before and after a wildfire: Comparison & implications. Geoderma, 261: 44-58. DOI:https://doi.org/10.1016/j.geoderma.2015.06.025

Kirkby, M.J., Gobin, A., Irvine, B., 2003. Pan European Soil Erosion Risk Assessment. Deliverable 5: PESERA Model Strategy, Land Use and Vegetation Growth, European Soil Bureau.

Kirkby, M.J., Irvine, B.J., Jones, R.J.A., Govers, G., THE PESERA TEAM, 2008. The PESERA coarse scale erosion model for Europe. I.–Model rationale and implementation. European Journal of Soil Science, 59(6): 1293-1306. DOI:https://doi.org/10.1111/j.1365-2389.2008.01072.x

Kirkby, M.J., Neale, R.H., 1987. soil erosion model incorporating seasonal factors, International Geomorphology,Part 2 (ed. V. Gardiner), pp. 189–210. Chichester: Wiley, c1987.

Le Bissonnais, Y., Daroussin, J.J., Jamagne, M., Lambert, J.J., Le Bas, C., King, D.D., Cerdan, O., Léonard, J.J., Bresson, L.-M., Jones, R.J.A., 2005. Pan-European soil crusting and erodibility assessment from the European Soil Geographical Database using pedotransfer rules. Advances in Environmental Modelling and Monitoring, 2(1): 1-15.

Li, E., 2016. Response of runoff and sediment to climate and human activities in the huangfuchuan watershed of the middle reaches of the yellow river. Doctoral Thesis, Northwest A&F University.

Li, J., Sun, R., Xiong, M., Chen, L., 2021a. Methodology of Time Series of Soil Erosion Dataset in Water Erosion Area of China in Five-year Increments (2000–2015). Journal of Global Change Data & Discovery, 5(02): 203-212+322-331. DOI:https://doi.org/10.3974/geodp.2021.02.13

Li, P., Chen, J., Zhao, G., Holden, J., Liu, B., Chan, F.K.S., Hu, J., Wu, P., Mu, X., 2022. Determining the drivers and rates of soil erosion on the Loess Plateau since. Science of the Total Environment, 823. DOI:https://doi.org/10.1016/j.scitotenv.2022.153674

Li, P., Holden, J., Irvine, B., Grayson, R., 2016a. PESERA-PEAT: a fluvial erosion model for blanket peatlands. Earth Surface Processes and Landforms, 41(14): 2058-2077. DOI:https://doi.org/10.1002/esp.3972

Li, P., Li, D., Hu, J., Fassnacht, F.E., Latifi, H., Yao, W., Gao, J., Chan, F.K.S., Dang, T., Tang, F., 2024. Improving the application of UAV-LiDAR for erosion monitoring through accounting for uncertainty in DEM of difference. Catena, 234: 107534. DOI:https://doi.org/10.1016/j.catena.2023.107534

Li, P., Mu, X., Holden, J., Wu, Y., Irvine, B., Wang, F., Gao, P., Zhao, G., Sun, W., 2017. Comparison of soil erosion models used to study the Chinese Loess Plateau. Earth-Science Reviews, 170: 17-30. DOI:http://dx.doi.org/10.1016/j.earscirev.2017.05.005

Li, P., Mu, X., Holden, J., Zhao, G., 2016b. Principles and applications of a coarse-scale soil erosion model, PESERA. Journal of Sedimentary Research(6): 74–80. DOI:https://doi.org/10.16239/j.cnki.0468-155x.2016.06.012

Li, P., Ren, F., Hu, J., Yan, L., Hao, M., Liu, L., Gao, J., Dang, T., 2023. Monitoring soil erosion on field

slopes by terrestrial laser scanning and structure-from-motion. Land Degradation & Development, 34(12): 3663-3680. DOI:https://doi.org/10.1002/ldr.4712

Li, P., Zang, Y., Ma, D., Yao, W., Holden, J., Irvine, B., Zhao, G., 2020. Soil erosion rates assessed by RUSLE and PESERA for a Chinese Loess Plateau catchment under land-cover changes. Earth Surface Processes and Landforms, 45(3): 707-722. DOI:https://doi.org/10.1002/esp.4767

Li, Y., Zhang, X., Cao, Z., Liu, Z., Lu, Z., Liu, Y., 2021b. Towards the progress of ecological restoration and economic development in China's Loess Plateau and strategy for more sustainable development. Science of The Total Environment, 756: 143676. DOI:https://doi.org/10.1016/j.scitotenv.2020.143676

Liu, B.Y., Nearing, M.A., Risse, L., 1994. Slope gradient effects on soil loss for steep slopes. Transactions of the ASAE, 37(6): 1835-1840. DOI:https://doi.org/10.13031/2013.28273

Liu, S., Liu, L., Liu, S., Lei, X., 2022. Characteristics and causal analysis of water and sediment changes in the qiaogou small watershed of the loess hilly gully region. Soil and Water Conservation in China(10): 9-15. DOI:https://doi.org/10.14123/j.cnki.swcc.2022.0242

Ma, J., Zeng, R., Yao, Y., Meng, X., Meng, X., Zhang, Z., Wang, H., Zhao, S., 2022. Characterization and quantitative evaluation of preferential infiltration in loess, based on a soil column field test. Catena, 213: 106164. DOI:https://doi.org/10.1016/j.catena.2022.106164

May, R.M., 1976. Simple mathematical models with very complicated dynamics. European Commission Joint Research Centre - IES, Ispra, Italy. NERC Centre for Ecology and Hydrology, Environment Centre Wales, Bangor, UK., 261(5560): 459-467. DOI:https://doi.org/10.1038/261459a0

McCool, D.K., Brown, L.C., Foster, G.R., Mutchler, C.K., Meyer, L.D., 1987. Revised slope steepness factor for the Universal Soil Loss Equation. Transactions of the ASAE, 30(5): 1387-1396. DOI:https://doi.org/10.13031/2013.30576

Miao, C., Zheng, H., Jiao, J., Feng, X., Duan, Q., Mpofu, E., 2020. The changing relationship between rainfall and surface runoff on the Loess Plateau, China. Journal of Geophysical Research: Atmospheres, 125(8): e2019JD032053. DOI: https://doi.org/10.1029/2019JD032053

Mondal, S., Mishra, A., 2024. Quantifying the precipitation, evapotranspiration, and soil moisture network's interaction over global land surface hydrological cycle. Water Resources Research, 60(2): e2023WR034861. DOI: https://doi.org/10.1029/2023WR034861

Nunes, A.N., de Almeida, A.C., Coelho, C.O.A., 2011. Impacts of land use and cover type on runoff and soil erosion in a marginal area of Portugal. Applied Geography, 31(2): 687-699. DOI:https://doi.org/10.1016/j.apgeog.2010.12.006

Osterkamp, W.R., Hupp, C.R., Stoffel, M., 2012. The interactions between vegetation and erosion: new directions for research at the interface of ecology and geomorphology. Earth Surface Processes and Landforms, 37(1): 23-36. DOI: https://doi.org/10.1002/esp.2173

Panagos, P., Borrelli, P., Robinson, D.A., 2015. Common Agricultural Policy: tackling soil loss across Europe. European Commission Joint Research Centre - IES, Ispra, Italy. NERC Centre for Ecology and Hydrology, Environment Centre Wales, Bangor, UK., Vol.526(No.7572): 195. DOI:https://doi.org/10.1038/526195d

Schmidt, S., Alewell, C., Meusburger, K., 2018. Mapping spatio-temporal dynamics of the cover

and management factor (C-factor) for grasslands in Switzerland. Remote Sensing of Environment, 211: 89-104. DOI:https://doi.org/10.1016/j.rse.2018.04.008

Shangguan, W., Dai, Y., Liu, B., Zhu, A., Duan, Q., Wu, L., Ji, D., Ye, A., Yuan, H., Zhang, Q., 2013. A China data set of soil properties for land surface modeling. Journal of Advances in Modeling Earth Systems, 5(2): 212-224. DOI: https://doi.org/10.1002/jame.20026

Sharpley, A.N., 1990. EPIC-erosion/productivity impact calculator: 1, Model Documentation. USDA Techn. Bull. 1759, 235. DOI:https://doi.org/10.5555/19911950112

Shi, P., Li, P., Li, Z., Sun, J., Wang, D., Min, Z., 2022. Effects of grass vegetation coverage and position on runoff and sediment yields on the slope of Loess Plateau, China. Agricultural Water Management, 259: 107231. DOI:https://doi.org/10.1016/j.agwat.2021.107231

Shi, W.-Y., Tateno, R., Zhang, J.-G., Wang, Y.-L., Yamanaka, N., Du, S., 2011. Response of soil respiration to precipitation during the dry season in two typical forest stands in the forest-grassland transition zone of the Loess Plateau. Agricultural and Forest Meteorology, 151(7): 854-863. DOI:https://doi.org/10.1016/j.agrformet.2011.02.003

Sun, C., Hou, H., Chen, W., 2021. Effects of vegetation cover and slope on soil erosion in the Eastern Chinese Loess Plateau under different rainfall regimes. Peerj, 9. DOI:https://doi.org/10.7717/peerj.11226

Sun, W., Shao, Q., Liu, J., Zhai, J., 2014. Assessing the effects of land use and topography on soil erosion on the Loess Plateau in China. Catena, 121: 151-163. DOI:http://dx.doi.org/10.1016/j.catena.2014.05.009

Tang, J., Sui, L., 2022. Geodetector-Based Livability Analysis of Potential Resettlement Locations for Villages in Coal Mining Areas on the Loess Plateau of China. Sustainability, 14(14): 8365. DOI:https://doi.org/10.3390/su14148365

Tang, J., Sui, L., Ma, T., Dan, Y., Yang, Q., Zhao, R., Qiang, X., 2023. GEE-Based Ecological Environment Variation Analysis under Human Projects in Typical China Loess Plateau Region. Applied Sciences, 13(8): 4663. DOI:https://doi.org/10.3390/app13084663

Trenberth, K.E., 1999. Conceptual framework for changes of extremes of the hydrological cycle with climate change. Climatic change, 42(1): 327-339. DOI:https://doi.org/10.1023/A:1005488920935

Valiantzas, J.D., 2013. Simplified forms for the standardized FAO-56 Penman–Monteith reference evapotranspiration using limited weather data. Journal of Hydrology, 505: 13-23. DOI:https://doi.org/10.1016/j.jhydrol.2013.09.005

Wang, L., 2017. Runoff-sediment coupling mechanism of different geomorphologic unit in the loess hilly-gully region. Doctoral Thesis, Northwest A&F University.

Wang, Z., Jiao, J., Rayburg, S., Wang, Q., Su, Y., 2016. Soil erosion resistance of “Grain for Green” vegetation types under extreme rainfall conditions on the Loess Plateau, China. Catena, 141: 109-116. DOI:http://dx.doi.org/10.1016/j.catena.2016.02.025

Wischmeier, W.H., Smith, D.D., 1978. Predicting rainfall erosion losses: a guide to conservation planning. Department of Agriculture, Science and Education Administration.

Wohler, L., Brouwer, P., Augustijn, D.C.M., Hoekstra, A.Y., Hogeboom, R.J., Irvine, B., Laemmchen, V., Niebaum, G., Krol, M.S., 2021. An integrated modelling approach to derive the grey water footprint of veterinary antibiotics. Environmental Pollution, 288.

DOI:https://doi.org/10.1016/j.envpol.2021.117746
Xin, Z., Xu, J., Zheng, W., 2008. Spatiotemporal variations of vegetation cover on the Chinese Loess Plateau (1981–2006): Impacts of climate changes and human activities. Science in China Series D: Earth Sciences, 51(1): 67-78. DOI:https://doi.org/10.1016/j.jhydrol.2013.09.005
Yu, X., Zhou, W., Chen, Y., Wang, Y., Cheng, P., Hou, Y., Wang, Y., Xiong, X., Yang, L., 2020. Spatial variation of soil properties and carbon under different land use types on the Chinese Loess Plateau. Science of the Total Environment, 703: 134946. DOI:https://doi.org/10.1016/j.scitotenv.2019.134946
Zhai, J., Wang, L., Liu, Y., Wang, C., Mao, X., 2023. Assessing the effects of China's Three-North Shelter Forest Program over 40 years. Science of the Total Environment, 857. DOI:https://doi.org/10.1016/j.scitotenv.2022.159354
Zhang, B., Zhang, G., Yang, H., Zhu, P., 2019. Temporal variation in soil erosion resistance of steep slopes restored with different vegetation communities on the Chinese Loess Plateau. Catena, 182: 104170. DOI:https://doi.org/10.1016/j.catena.2019.104170
Zhang, H., Wang, B., Li Liu, D., Zhang, M., Leslie, L.M., Yu, Q., 2020. Using an improved SWAT model to simulate hydrological responses to land use change: A case study of a catchment in tropical Australia. Journal of Hydrology, 585: 124822. DOI:https://doi.org/10.1016/j.jhydrol.2020.124822
Zhang, X., Song, J., Wang, Y., Sun, H., Li, Q., 2022. Threshold effects of vegetation coverage on runoff and soil loss in the Loess Plateau of China: A meta-analysis. Geoderma, 412: 115720. DOI:https://doi.org/10.1016/j.geoderma.2022.115720
Zhang, Y., Chen, Y., 2020. Research trends and areas of focus on the Chinese Loess Plateau: A bibliometric analysis during 1991–2018. Catena, 194: 104798. DOI:https://doi.org/10.1016/j.catena.2020.104798
Zhao, G., Mu, X., Han, M., An, Z., Gao, P., Sun, W., Xu, W., 2017. Sediment yield and sources in dam-controlled watersheds on the northern Loess Plateau. Catena, 149: 110-119. DOI:https://doi.org/10.1016/j.catena.2016.09.010
Zhao, G., Mu, X., Wen, Z., Wang, F., Gao, P., 2013. Soil erosion, conservation, and eco-environment changes in the Loess Plateau of China. Land Degradation & Development, 24(5): 499-510. DOI:https://doi.org/10.1002/ldr.2246
Zhao, J., Vanmaercke, M., Chen, L., Govers, G., 2016. Vegetation cover and topography rather than human disturbance control gully density and sediment production on the Chinese Loess Plateau. Geomorphology, 274: 92-105.
Zhao, J., Wang, Z., Dong, Y., Yang, Z., Govers, G., 2022a. How soil erosion and runoff are related to land use, topography and annual precipitation: Insights from a meta-analysis of erosion plots in China. Science of the Total Environment, 802: 149665. DOI:https://doi.org/10.1016/j.scitotenv.2021.149665
Zhao, J., Wang, Z., Dong, Y., Yang, Z., Govers, G., 2022b. How soil erosion and runoff are related to land use, topography and annual precipitation: Insights from a meta-analysis of erosion plots in China. Science of the Total Environment, 802. DOI:https://doi.org/10.1016/j.scitotenv.2021.149665
Zhou, Y., Marshall, L., Li, D., Sharma, A., 2024. Revisiting evapotranspiration inputs in eco-

hydrological modeling for climate change assessment. Journal of Hydrology: 131888. DOI:https://doi.org/10.1016/j.jhydrol.2024.131888

Zhu, B., Zhou, Z., Li, Z., 2021. Soil erosion and controls in the slope-gully system of the Loess Plateau of China: A review. Frontiers in Environmental Science, 9: 136. DOI:https://doi.org/10.3389/fenvs.2021.657030